

Process simulation for the 1990s

H. Stippel, E. Leitner, Ch. Pichler,
H. Puchner, E. Strasser and S. Selberherr

Institute for Microelectronics, Technical University of Vienna, Gusshausstraße 27–29, A-1040 Vienna, Austria (email: stippel@iue.tuwien.ac.at)

In this paper, an outlook on future aspects of process simulation is given. The main direction for ongoing research is simulation in three space dimensions. For modern devices, all three spatial coordinates must be obeyed in process simulation, to provide sufficiently accurate doping profiles and device geometry for three-dimensional device simulation and, therefore, to predict the electric behaviour of the device realistically. Some new techniques to circumvent current limitations in three-dimensional process simulations are depicted. Aspects of process flow representation for future automatic process optimization are discussed.

1. Introduction

The miniaturization of today's semiconductor devices suggests a change from the common two-dimensional layout to three-dimensional structures to increase the number of devices per unit wafer area. New technologies are being developed to cover the continuously growing demands for the production of those new structures. Therefore, modern process simulators must be capable of modelling arbitrarily complex three-dimensional geometries.

For simulation of the electrical behaviour of such new devices, three-dimensional device simulators exist, emanating from universities as well as from commercial sources. The required information about the three-dimensional doping profiles is

usually developed from either analytic models or from rotations and stretching of doping profiles generated by two-dimensional process simulations. Three-dimensional process simulation would be useful for analysing realistic three-dimensional structures, as well as for providing more accurate doping profiles as input for three-dimensional device simulators. Currently, no well established and widely available three-dimensional process simulators exist. Consequently, this will be a key goal for future research activities.

As has already been pointed out [1], there are two major problems for three-dimensional simulations: first, three-dimensional computations are very CPU-time intensive; second, in some fields (e.g. for diffusion processes), there is simply a lack of really good and accurate models. In this paper, emphasis is put on our approaches for numerical solutions and methods to accelerate three-dimensional process simulation, as well as on general state-of-the-art process simulation. The development of new, more physically-based models is only briefly incorporated in this paper, because such efforts require accurate three-dimensional measurements, whereas in reality, hardly any satisfactory two-dimensional measurements exist [1]. A better understanding of the physics behind the bulk processes demands further improvements in metrology.

Just recently, more and more emphasis is being placed on the coupling of different process simulators in order to be able to model a real process accurately [2]. Moreover, optimization of processes for a desired electrical behaviour of a device is becoming a key topic in modern process and technology development. This increasing importance of simulator coupling and process optimization is also an area for future research activities.

2. Topography simulation

Topography simulation deals with the basic processes of pattern definition and pattern transfer, which ultimately change the shape of the wafer surface. The numerical algorithms for surface movement play a key role in those simulators, and lead to major differences in the accuracy, robustness and efficiency of the simulation tools. Historically, it has often been sufficient to simulate only the two-dimensional cross-section of an integrated device feature. Programs like SAMPLE [3, 4], SPEEDIE [5] or COMPOSITE [6] use the well-known string algorithm [7] for fast and accurate computation of two-dimensional topography processes. These programs are widely available, and are applied with great success. However, the real problems are in three-dimensional topography simulation.

A variety of surface evolution algorithms has been studied to build three-dimensional topography simulators. Basically, there are two types of algorithms used for modelling three-dimensional topography processes. Volume removal methods divide the material being etched into a large array of rectangular prismatic cells. Each cell is characterized as etched, unetched or partially etched. During etching, cells are removed one-by-one according to the local etch rate and the number of cell faces exposed to the etching medium. These algorithms have been successfully used in three-dimensional lithography simulation [8–10]. Cell-removal methods can easily handle arbitrary geometries, but

unfortunately they suffer from inherent inaccuracy, because they favour certain etch directions [10]. Surface advancement methods, on the other hand, represent the surface of the material being etched by using a mesh of points which are connected by line segments to form triangular facets [11]. Depending on the implementation, either the mesh points or the facets are moved according to the local etch rates. A mesh management is necessary to maintain the mesh as it moves in time. In general, surface advancement algorithms offer highly accurate results, though with potential topological instabilities such as erroneous surface loops which result from a growing or etching surface intersecting with itself. The surface loops must be removed before they become too complex, which is a rather complicated task in three-dimensional simulation [12].

Our method for surface movement is a new approach [13, 14]. It is based on fundamental morphological operations used in image and signal processing [15], and allows accurate simulation of arbitrary three-dimensional structures without loop formation. The simulation geometry is basically considered as a two-valued image (material or vacuum). Figure 1a illustrates the material representation of the simulation tool. We use an array of square or cubic cells, where each cell is characterized as etched or unetched. Additionally, a material identifier is defined for each cell, therefore material boundaries need not be explicitly represented. The surface or etching boundary consists of unetched cells that are in contact with fully etched cells. Cells on the surface are exposed to the etching medium or to the deposition source, and etching or deposition proceeds on this surface. A linked surface cell list stores dynamically etch or deposition rates of exposed cells. To advance the etch front, spatial filter operations based on the erosion or dilation operation [15] are performed along the surface boundary, as shown in Fig. 1a and Fig. 1b. During an etching process, all cells within a filter are etched away, while cells

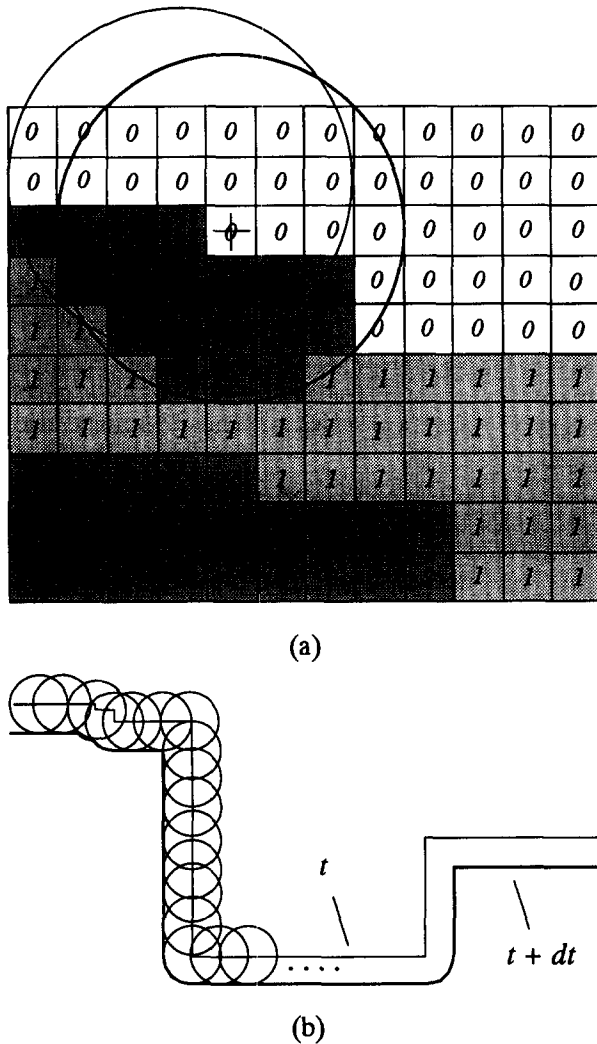


Fig. 1. Material representation of the topography simulation tool.

outside stay unchanged. Usually, for anisotropic three-dimensional simulations, filters are ellipsoids, and for isotropic movement of surface points filters are spheres, although there is no restriction on the filter shape. The spatial dimension of an applied filter determines how far a surface point moves. The main axes of an ellipsoid are given by the local etch or deposition rates multiplied by the time step. After each time step the exposed boundary has to be determined.

Therefore, all the cells in the material are scanned. Material cells are surface cells if at least one cell side is in contact with an already etched cell. The exposed sides of the detected surface cells describe the etch or deposition front at a certain time step.

When the surface passes from one material to another, filter operations must be performed by using composite filters. The important question is how the surface evolves at the boundary, since interfaces lead to an abrupt change in etch rates. Therefore, filter operations are performed selectively on a given material. That means filter operations on cells of a given material will only remove cells of the same material. If a filter extends over a material boundary, it demands an additional filter operation performed selectively on the second material. The etch rate for this second filter operation is calculated regarding the etch rates on both sides of the interface, and depending on how far the filter reaches into the other material.

Many processes are strongly affected by the shape of the surface. Modelling of realistic etching and deposition processes requires information about the shadowing of surface points and local surface orientation. Additionally, some surface regions will have a restricted view of the 'sky' above the wafer which, for instance, determines the amount of incoming flux during a sputter deposition process. To calculate realistic etch or growth rate distributions, an efficient shadow test has been implemented to determine if a cell on the surface is shadowed by other cells or not. The problem of whether a certain part of the sky is visible from a viewing point on the surface can be reduced to a series of shadow tests. The 'sky' is divided up into several parts, and a shadow test determines if a part is visible from a given surface point or not. All this information is used to calculate the etch or growth rate distribution along the surface boundary, starting from a primary given rate. The calculated etch or growth rate distribution and the

angular flux distribution of incoming species in turn influences the shape and direction of the applied filters, and thereby the evolution of the wafer surface.

In Fig. 2 the result of sequential etching processes to simulate three-dimensional contact hole etching is shown. The simulation for this example starts with a circular mask opening of 1 micrometer in diameter. The first isotropic etching process etches the substrate to a depth of 0.5 microns. The spatial filter for the isotropic etching step is a sphere. The etching rate for this step is 0.03 microns per minute. The etching time was 1000 seconds, simulated with time steps of 250 seconds. This isotropic etching process is followed by a directional etching step for 0.5 micrometer of additional material removal. The directional etch rate is 0.040 microns per minute, and the isotropic etch rate is 0.008 microns per minute. The etching time for the directional etching step was 800 seconds, simulated with time steps of 200 seconds. The number of cells for this example was 100 cells per micron in each direction; the calculation time was 43 minutes.

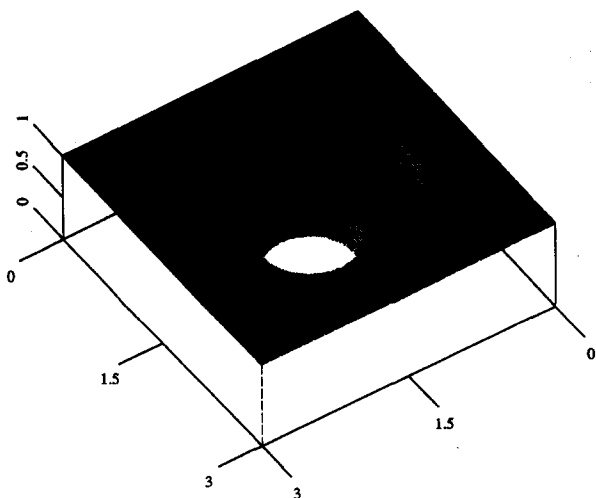


Fig. 2. Simulation of contact hole etching.

3. Ion implantation

Ion implantation is currently the most important technique for introducing dopants into semiconductors. As modern annealing methods (RTA) do not alter the implanted profile very much anymore, the determination of the initial implantation profile has become a very important task. Thus, the simulation of ion implantation has gained in significance tremendously. For the simulation, three main techniques can be used: the analytical description of the doping profile [16, 17], the solution of the Boltzmann transport equation [18] or the Monte Carlo method [19–21].

The analytical method usually has the advantage of minor demands on CPU-time consumption. One-dimensional profiles can be modelled accurately by the analytical description of profiles. For two-dimensional computations, though, problems already arise, because of the lack of an underlying physical base for multi-dimensional extensions of this technique. The limitations can be seen on examples with abrupt changes of the simulation geometry or for tilted implantations. Examples for these restrictions can be found elsewhere [22, 23]. Finally, in the three-dimensional space, the CPU-time requirements increase dramatically, and this last advantage, against the other mentioned methods, loses its weight.

The solution of the Boltzmann transport equation is very efficient and accurate for one-dimensional applications [24]. For two-dimensional simulations, the CPU-time and memory requirements increase significantly. Nevertheless, this method can be still advantageous compared to the two-dimensional Monte Carlo methods, when demands on accuracy are not too high. For three-dimensional simulations, this method is, despite today's computer power, inapplicable.

For the above-listed reasons, the Monte Carlo method is the choice for three-dimensional

problems, although some special considerations are necessary to reduce the otherwise tremendous CPU-time consumption. Two main techniques have been developed to accelerate the simulation: first a superposition method is used to decrease the number of collision events to be evaluated [21]; second, an octree has been introduced for the discretization of the geometry to simplify the point location problem [25].

For the superposition method, a model trajectory is first computed for each material in the simulation area, and then this model trajectory is copied several times into the simulation window. Using this technique, from a few thousand model trajectories about a million physical trajectories can be derived. In this manner, the number of collision event evaluations, and therefore the CPU-time consumption, are decreased. However, the computation time required for the necessary geometry checks for the point location remains the same. To decrease this time an octree discretization has been adapted to the needs of the ion implantation.

The octree method comes from graphical image processing [26]. For this method, a cube (the root cube) is constructed first, containing the entire simulation area. This cube is then subdivided into eight subcubes. This procedure is recursively continued for every subcube until either the desired accuracy of the discretization is reached or no more intersections of this cube with the polygons defining the target geometry exist. For every leaf-cube the material which it contains is determined; one leaf can only contain one material. Later, then, for the point location simple inequality comparisons can be used. The octree is stored as a tree in the memory, as can be seen in Fig. 3. This method speeds up the simulation tremendously. The computation time required for one trajectory is the same as for two-dimensional simulations.

Another problem is the incorporation of the real crystalline structure of semiconductor materials. Although crystalline simulators exist [27], the

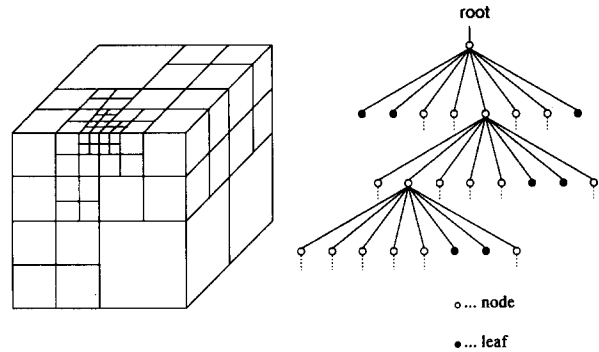


Fig. 3. Discretization using an octree.

time required to get three-dimensional results is very high, because the superposition method cannot be used for crystalline targets. But from Fig. 4, it can be seen that the effect of a crystalline target has to be taken into account: Boron was implanted with a tilt angle of 0° and an energy of 30 keV into an amorphous target (Fig. 4a) and a crystalline one (Fig. 4b). There is a significant difference in the mean projected range. The ions penetrate the crystalline target about twice as deep as the amorphous material.

Transient computations, including damage, are even more time-expensive, and only initial attempts are known as yet [28]. Future work on ion implantation needs to include even more efficient algorithms for these computations. Also, migration to highly parallel computers should be taken into account.

4. Diffusion

Modelling dopant diffusion processes in various target materials is a major task in process simulation. Rigorous diffusion models must incorporate various concepts. In 1974, Hu [29] introduced the dual diffusion mechanism for silicon, involving the lattice vacancy and the silicon self-interstitial for mediating the dopant diffusion. Oxidation enhanced/retarded diffusion [30] and retarded diffusion during thermal nitridation [31] and silicidation [32] are compatible

with the dual mechanism. In recent years, pair diffusion [33–36] advanced in diffusion model-

ling by hypothesizing that dopant diffusion proceeds by dopant point-defect pairs. High concentration effects like clustering and precipitation are inherently connected to the processes of activation and deactivation of dopants [37, 38], and are still not well understood.

In this work, the basic equations and an example of a new diffusion model are first shown, and then the numerical aspects are discussed.

4.1 Modelling diffusion processes

Modelling realistic diffusion processes requires the incorporation of as much physics as possible to obtain sufficient accuracy. To design a new simulation model, one has to make a compromise between the number of parameters and the underlying physical relationships. As an example, a robust, physically-based model which is easy to understand is presented below in the form of a two-dimensional simulation model for dopant diffusion in polysilicon.

Polysilicon layers are used in modern IC fabrication processes as diffusion sources, for instance, for out-diffusion processes by forming an n-polysilicon-gate MOSFET, or for emitter and graft-base formation in high performance bipolar LSI technology [39]. Any advanced polysilicon diffusion model must include various phenomena such as clustering due to the excessively high dopant concentrations and segregation kinetics, to handle the exchange of dopants in the grain/grain-boundary network. To determine the impurity profile in the complex lattice polysilicon-silicon structure, it is also necessary to include a generation/recombination mechanism and grain growth kinetics. The two-dimensional coupled PDEs for the active dopant concentration in the grain interior (C_{ga}) and the grain boundaries (C_{gb}) are given in eqs. (1)–(3), where s denotes the charge state of the dopant and r is the effective grain size, which can be seen as the reciprocal grain boundary area per unit volume, γ denotes a geometric factor taking into

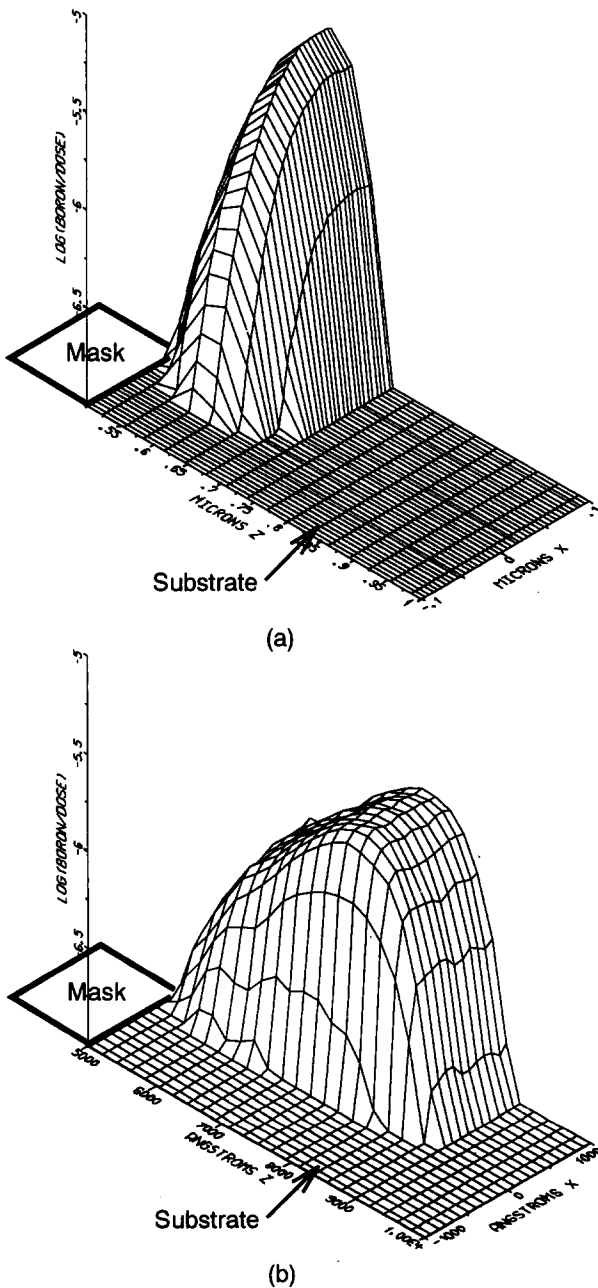


Fig. 4. Comparison between amorphous and crystalline results.

account the structure of the polysilicon material. Diffusion and segregation kinetics is followed after [40]:

$$\frac{\partial C_{ga}}{\partial t} = \text{div} \left(D_{ga} \left(\text{grad } C_{ga} + s \cdot \frac{C_{ga}}{U_T} \cdot \text{grad } \psi \right) \right) - G_{seg} \quad (1)$$

$$\frac{\partial C_{gb}}{\partial t} = \text{div} \left(\gamma \cdot D_{gb} \left(\text{grad } C_{gb} + \frac{C_{gb}}{r} \cdot \text{grad } r \right) \right) + G_{seg} \quad (2)$$

$$G_{seg} = t \cdot \left(\frac{T_b^{\max}}{r} - C_{gb} \right) \cdot C_{ga} - e \cdot (C_g^{\text{sol}} - C_{ga}) \cdot C_{gb} \quad (3)$$

Equation (3) describes the generation/recombination term of the exchange of dopants between grain interiors and grain boundaries by the use of trapping t and emission e factors, where T_b^{\max} denotes the maximum number of free states in the grain boundary. C_g^{sol} is the solubility limit for the dopant species; it is also taken to calculate the active grain interior concentration C_{ga} from the total interior concentration C_g^t in the static clustering model, eq. (4) (after [41]):

$$\frac{C_g^t}{C_g^{\text{sol}}} = \frac{C_{ga}}{C_g^{\text{sol}}} + m_g \cdot \left(\frac{C_{ga}}{C_g^{\text{sol}}} \right)^{2 \cdot m_g} \quad (4)$$

During the thermal treatment, grain growth occurs. In this model, the grains of polysilicon are assumed to be squares ($\gamma = 1$), growing from initial grain size r_0 . Calculation of the migration of the grain boundaries is based on thermodynamic concepts of surface energy anisotropy and secondary grain growth [42, 43]. From basic rate theory, the net rate of atomic transfer of dopants from lattice sites from one grain to those of a neighbour site is given by a complementary Arrhenius law

$$\Delta K = K^+ \cdot (1 - e^{-\frac{\Delta\mu}{kT}}) \quad (5)$$

where K^+ denotes a jump frequency for atoms at the boundary, and $\Delta\mu$ is the difference in the electrochemical potential on either site of the boundary. Under constant pressure and volume, the electrochemical potential is given by eq. (6). The boundary migration G is obtained from eq. (7):

$$\Delta\mu = \frac{\Delta F \cdot \bar{V}}{N} \quad (6)$$

$$G = \lambda \cdot \Delta K \quad (7)$$

N denotes Avogadro's number, \bar{V} denotes the atomic volume, ΔF the change in Helmholtz free energy, and λ the thickness of the boundary. The jump frequency K^+ can be expressed in terms of the temperature dependent diffusivity; thus the growth rate reads:

$$\frac{\partial r}{\partial t} = \frac{D_{ga}}{\lambda} \cdot [1 - e^{-\frac{\Delta\mu}{kT}}] \quad (8)$$

The grain growth depends upon the local dopant concentration via the diffusion coefficient D_{ga} , so the grain size becomes non-uniform along the vertical and lateral directions.

Figure 5 shows the simulation results for an outdiffusion process of arsenic from a $0.6 \times 0.1 \mu\text{m}$ poly-layer in a mono-Si substrate. By using such a thin poly-layer, a characteristic dopant pile-up at the mono-Si/poly interface takes place, and influences the outdiffused concentration in the substrate. In our simulations, the interface is treated like a special grain boundary with a smaller number of free states and a higher trapping rate, due to the thin interfacial oxide layer.

4.2 The numerical view on diffusion

Major tasks for solving the PDEs for diffusion are gridding, discretization and solving the

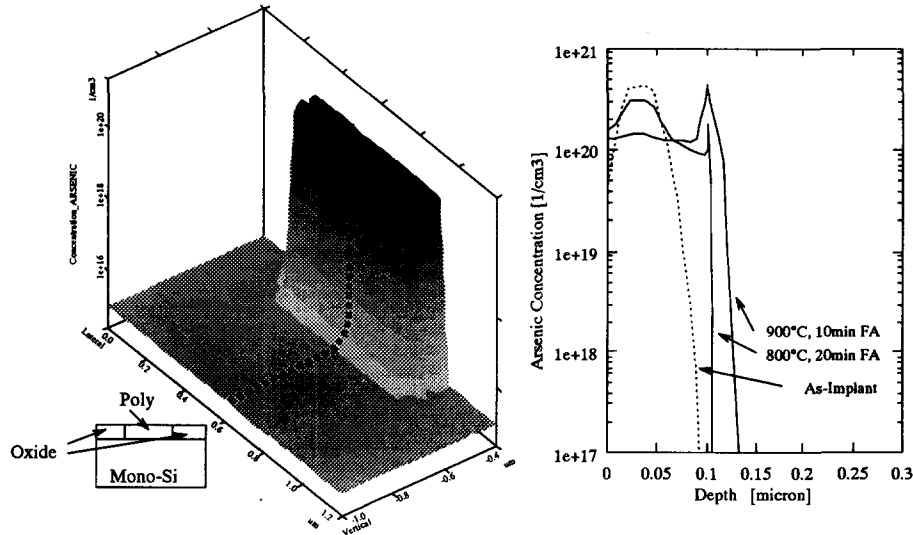


Fig. 5. Poly-out-diffusion of arsenic for 900°C 10 min. FA. and 800°C 20 min. FA. Simulations agree with SIMS measurements [39].

nonlinear system of equations. Although these topics influence each other, they can be treated separately.

For gridding, the main problem is the complex structures that have to be treated. In some cases, the simulation within the silicon layer with respective gridding of the silicon region is sufficient. However, often it is necessary to take more regions into account, e.g. in the above-mentioned model, the polysilicon and crystalline regions need to be gridded together. Critical points for grid generation and adaption are:

- The boundaries and internal interfaces (e.g. the poly/crystalline boundary) have to be resolved with a sufficient accuracy. This implies a controllable density distribution of gridpoints either according to empirical functions or based on discretization error estimates.
- As the diffusion front advances, the density distribution varies with time, which requires a grid adaption between subsequent timesteps,

and an interpolation of the quantities computed.

- To maintain good numerical behaviour of the nonlinear system, grid elements have to obey certain quality criteria, e.g. geometric or Delaunay conditions.

For spatial discretization two methods are widely used: finite differences and finite elements. The finite element method is more general; from the mathematical point of view, the finite differences are just a special case of finite elements with a particular weighting function [44]. Convective terms in the partial differential equation, like the influence of the electrostatic potential or grid-point velocities in moving boundary problems, can be treated through directional weighting functions, as shown elsewhere [44]. This leads to the same results as obtained by the Scharfetter-Gummel approach with finite differences [45].

Especially important for three-dimensional approaches is that finite elements require less restrictive criteria for the grid elements, because

fulfilment of the Delaunay condition [44] is not necessary (although desirable), which simplifies grid generation.

Currently, our two-dimensional process simulator PROMIS uses finite differences based on a transformed orthoproduct grid. For highly nonplanar structures and heavy nonlinearity of diffusion equations, the computational stability is, however, quite poor. The reason is that the connectivity of the grid does not represent the actual coupling of the gridpoints, because the Delaunay condition is not fulfilled. Future work will make use of more general triangular grids combined with finite elements.

Very important for solving the partial differential equations is the time discretization and time integration for the coupled system of ordinary nonlinear differential equations, obtained through spatial discretization. For time discretization the finite differences method is state-of-the-art [44]. In PROMIS the size of the time-steps is controlled adaptively. The adaption is based on the time discretization error and the nonlinearity of the coefficients of the differential equations. To prevent oscillations, a nonlinear damping scheme for the predicted value is used.

The traditional way to solve the nonlinear system of coupled equations at each timestep is to use fully coupled, Newton-like methods. These exhibit very good convergence behaviour, even for strongly coupled equations. Decoupled schemes [46, 47], like Gummel's method or nonlinear Gauss-Seidel iteration, often diverge.

Alternatively, Krylov methods [48] may be used, where matrix free iterations are performed. These methods seem promising, because of their low memory requirements. However, problems arise from preconditioning.

Competitive solutions for nonlinear systems using multigrid methods have been shown [49, 50]. These methods exhibit excellent

convergence behaviour which does not depend upon gridspacing. Although it is possible to apply this method on unstructured grids, such an approach is currently unknown, and might be considered for future activities.

For the solution of linear systems, iterative techniques allow us to solve systems of a very high order, but they live and die with preconditioning. Recent work [51] shows that even for large systems with a relatively high bandwidth arising from three-dimensional problems, solutions are possible within an acceptable time. It has been demonstrated [52] that for two-dimensional problems with structural symmetry, direct solvers are computationally competitive. For three dimensions their memory requirements are far too high, so that no practical use is given.

PROMIS uses a BiCGStab algorithm with an incomplete Gauss preconditioner [51], which is about ten times as fast as an optimal SOR algorithm.

5. Process flow integration

The manufacturing of a semiconductor wafer may require several hundred processing steps, and may take several weeks to complete. During the design stages of a device, a large number of experiments have to be made to determine appropriate settings of certain process parameters, as well as of the layout's topology and the geometrical dimensions best suited to meet the device specifications. Depending on the nature of the device feature under consideration, iteration and optimization loops may comprise process simulation sequences of any length.

For each particular fabrication process step, a variety of simulation tools exist [3, 4, 14, 53, 54] which provide an easy means for investigating the response to changes in parameter values without actually going to the production line. All of these tools are more or less specific about the representation of wafer data on the one hand, and

about their control arguments on the other hand. Therefore, numerous efforts have to be made with respect to data conversion, tool calibration and parameter translation, which make the use of such a tool a highly specialized task in itself.

Supporting the process and device engineers in an efficient and intuitive way in exploring the design space calls for a number of capabilities of the process simulation environment:

- *Dynamic attention focus* to allow free interaction with, and analysis of, all aspects of a device.
- *Data transparency* with respect to real-life data; *data hiding* with respect to computation-induced data.
- *Data tracking and revision control* to facilitate the management of large-scale and iterative experiments.
- *Computation hiding* to liberate the user from all details of the generation of numerical data, including the selection of appropriate tools.
- *Portability, communicability and modularization of recipes* to pave the way for technology knowledge sharing and remote fabrication, as well as to encourage the reuse of existing results.
- *Intuitive man-machine interface, documentation facilities.*

Several contributors have been made to this goal [55–60]. However, no single solution exists that satisfactorily covers all the issues mentioned above.

Within VISTA [61], tool integration activities resulted in a simulation flow control module [62] that allows the specification of process sequences by means of simulator calls used in a plug-and-play-fashion. A subset of the Profile Interchange Format (PIF) [63] is used as the basis for an unambiguous wafer state description [64].

The integration of independently developed simulators is achieved by providing a binding function that makes the tool available to the TCAD framework. Process flows may either be defined by writing a text file using symbolic names for the simulators to invoke, or by using a graphical process flow editor. Code-reuse is supported by a module inclusion mechanism that allows for recursive parameter overriding. All intermediate results stay available for analysis at a later time, unless they are removed explicitly. The following example shows the definition of a modern low-voltage CMOS process as a sequence of PROMIS simulator module calls. The oxidation step was replaced by a deposition step:

```
(
  (monte-carlo-implant :niond 1000 :dose 1e12 :nelem 5 :energy 160.)
  (diffuse :planar T)
  (unidirectional-deposition :material ("SiO2" 0.004) :simulation-time 300.)
  (unidirectional-deposition :material ("POLYSILICON" 0.16)
    :simulation-time 300.)
  (spin-on :material "Resist" :thickness 1.)
  (expose :mask ((0.5 1.5)) :invert T)
  (isotropic-etch :material (("Resist" 0.02) ("Exposed" 0.22) ("SiO2" 0.0)))
  (plasma-etch :material (("POLYSILICON" 0.0 0.2)
    ("SiO2" 0.0 0.0) ("Si" 0.0 0.0)))
  (isotropic-etch :material (("Resist" 0.22) ("POLYSILICON"
    ("SiO2" 0.0) ("Si" 0.0)))
  (monte-carlo-implant :niond 1000 :dose 1e13 :nelem 15 :energy 10.)
  (diffuse :planar T)
  (isotropic-deposition :material ("SiO2" 0.04))
  (plasma-etch :material (("SiO2" 0.0 0.045)
    ("POLYSILICON" 0.0 0.0) ("Si" 0.0 0.0)))
  (unidirectional-deposition :material ("WSi2" 0.04))
  (isotropic-etch :material (("WSi2" 0.01) ("SiO2" 0.0)))
)
```

Note that only those tool parameters are specified which are significant to the process; all other simulator keys are taken from default value tables. By switching between such tables at run-time, simulator behaviour may be modified without affecting user settings.

Drawing on these first results, we are going to move from a LISP-based implementation to a C-LISP-hybrid, define a tool integration policy which allows for the automatic generation of binding code, and add lot-split and lot-merge capabilities. Moreover, interfaces with a database system and with a knowledge-based system to capture process and device design information and expertise are to be established.

6. Conclusion

In this paper, state-of-the-art process modelling has been outlined. Moreover, future trends for the process simulation have been discussed. Those developments include the extension of simulators to three-dimensional structures, in terms of new models, and to automatic consecutive invocation of different simulators, including process optimization.

For those key points, current limitations were highlighted and approaches for solutions were shown. But the main problem is still the metrology. As there are no accurate two-dimensional measurements yet available, the development of more accurate models or even three-dimensional simulation tools suffers from the lack of both understanding the really basic physics as well as the missing possibility for the verification of the results by comparing them to experimental data.

Acknowledgements

This project is supported by the laboratories of: Austrian Industries – AMS at Unterpremstätten, Austria; Digital Equipment Corporation at Hudson, USA and Siemens Corporation at Munich, Germany.

References

- [1] M.E. Law, Challenges to achieving accurate three-dimensional process simulation, *SISDEP 93*, 1993, 1–8.
- [2] F. Fasching, S. Halama and S. Selberherr, editors, *Technology CAD Systems*, Springer, 1993.
- [3] W.G. Oldham, S.N. Nandgaonkar, A.R. Neureuther and M.M. O'Toole, A general simulator for VLSI lithography and etching processes: Part I – Application to projection lithography, *IEEE Trans. Electron Dev.*, 26 (1979) 717–722.
- [4] W.G. Oldham, A.R. Neureuther, C. Sung, J.L. Reynolds and S.N. Nandgaonkar, A general simulator for VLSI lithography and etching processes: Part II – Application to deposition and etching, *IEEE Trans. Electron Dev.*, 27 (1980) 1455–1459.
- [5] J. McVittie, J. Rey, L.Y. Cheng, A. Bariya, S. Ravi and K. Saraswat, SPEEDIE: A profile simulator for etching and deposition, *TECHNOCON*, 1990, 16–19.
- [6] J. Lorenz, J. Pelka, H. Ryssel, A. Sachs, A. Seidel and M. Svoboda, COMPOSITE – A complete modeling program of silicon technology, *IEEE Trans. Computer-Aided Des. Integrated Circuits and Syst.*, 4(4) (1985) 421–430.
- [7] R.E. Jewett, P.I. Hagouel, A.R. Neureuther and T. Van Duzer, Line-profile resist development simulation techniques, *Polymer Eng. Sci.*, 17(6) (1977) 381–384.
- [8] E.W. Scheckler, K.K.H. Toh, D.M. Hoffstetter and A.R. Neureuther, 3D lithography, etching, and deposition simulation (SAMPLE-3D), *1991 Symposium on VLSI Technology*, 1991, 97–98.
- [9] W. Henke, D. Mewes, M. Weiß, G. Czech and R. Schließl Hoyer, A study of reticle defects imaged into three-dimensional developed profiles of positive photoresists using the SOLID lithography simulator, *Microelectronic Eng.*, 14 (1991) 283–297.
- [10] Y. Hirai, S. Tomida, K. Ikeda, M. Sasago, M. Endo, S. Hayama and N. Nomura, Three-dimensional resist process simulator PEACE (Photo and Electron Beam Lithography Analyzing Computer Engineering System), *IEEE Trans. Computer-Aided Design Integrated Circuits and Syst.*, 10(6) (1991) 802–807.
- [11] E.W. Scheckler, Algorithms for three-dimensional simulation of etching and deposition processes in integrated circuit fabrication, *PhD thesis*, University of California, Berkeley, 1991.
- [12] J.J. Helmsen, E.W. Scheckler, A.R. Neureuther and C.H. Séquin, An efficient loop detection and removal algorithm for 3D surface-based lithography simulation, *NUPAD IV*, 1992, 3–8.
- [13] E. Strasser, K. Wimmer and S. Selberherr, A new method for simulation of etching and deposition processes, *VPAD 93*, 1993, 54–55.
- [14] E. Strasser and S. Selberherr, A general simulation method for etching and deposition processes, *SISDEP 93*, 1993, 357–360.
- [15] C.R. Giardina and E.R. Dougherty, *Morphological Methods in Image and Signal Processing*, Prentice-Hall, 1988.
- [16] J.F. Gibbons, Ion implantation in semiconductors – Part I: Range distribution theory and experiments, *Proc. IEEE*, 56(3) (1968) 295–313.
- [17] H. Ryssel, G. Prinke and K. Hoffmann, Implantation and diffusion models for process simulation, *VLSI Process and Device Modeling*, 1983, 1–41.
- [18] L.A. Christel, J.F. Gibbons and S. Mylroie, An application of the Boltzmann transport equation to ion range and damage distribution in multilayered targets, *J. Appl. Physics*, 51(12) (1980) 6176–6182.
- [19] M.T. Robinson and O.S. Oen, Computer studies of

- the slowing down of energetic atoms in crystals, *Physical Rev.*, 132(6) (1963) 2385–2398.
- [20] J.F. Ziegler, J.P. Biersack and U. Littmark, *The Stopping and Range of Ions in Solids*, Pergamon Press, 1985.
 - [21] G. Hobler and S. Selberherr, Monte Carlo simulation of ion implantation into two- and three-dimensional structures, *IEEE Trans. Computer-Aided Design Integrated Circuits and Syst.*, 8(5) (1989) 450–459.
 - [22] G. Hobler, Simulation der Ionenimplantation in ein-, zwei- und dreidimensionalen Strukturen, *PhD thesis*, Technische Universität Wien, Austria, 1988.
 - [23] H. Stippel, Simulation der Ionen-Implantation, *PhD thesis*, Technische Universität Wien, Austria, 1993.
 - [24] M.D. Giles, Ion implantation calculations in two dimensions using the Boltzmann transport equation, *IEEE Trans. Computer-Aided Design Integrated Circuits and Syst.*, 5(4) (1986) 679–684.
 - [25] H. Stippel and S. Selberherr, Three dimensional Monte Carlo simulation of ion implantation with octree based point location, *VPAD 93*, 1993, 122–123.
 - [26] M. Mäntylä, *An Introduction To Solid Modeling*, Computer Science Press, 1988.
 - [27] G. Hobler, H. Pötzl, L. Gong and H. Ryssel, Two-dimensional Monte Carlo simulation of boron implantation in crystalline silicon, *SISDEP 91*, 1991, 389–398.
 - [28] A. Simionescu and G. Hobler, Two dimensional Monte Carlo simulation of ion implantation in crystalline silicon considering damage formation, *SISDEP 93*, 1993, 361–364.
 - [29] S.M. Hu, Formation of stacking faults and enhanced diffusion in the oxidation of silicon, *J. Appl. Physics*, 45(4) (1974) 1567–1573.
 - [30] D.A. Antoniadis and I. Moskowitz, Diffusion of substitutional impurities in silicon at short oxidation times: an insight into point defect kinetics, *J. Appl. Physics*, 53(10) (1982) 6788–6796.
 - [31] S. Mizuo and H. Higuchi, Effect of back-side oxidation on B and P diffusion in Si directly masked with Si₃N₄ films, *J. Electrochem. Soc.: Solid-State Science and Technology*, 129(10) (1982) 2292–2295.
 - [32] K. Maex and L. Van Den Hove, The effect of silicides on the induction and removal of defects in silicon, *Materials Sci. Eng.*, B 4 (1989) 321–329.
 - [33] F.F. Morehead and R.F. Lever, Enhanced tail diffusion of phosphorus and boron in silicon, *Appl. Physics Lett.*, 48(2) (1986) 151–153.
 - [34] R.B. Fair, Shallow junctions – Modeling the dominance of point defect charge states during transient diffusion, *Int. Electron Devices Meeting*, 1989, 691–694.
 - [35] B.J. Mulvaney and W.B. Richardson, Physical models for impurity diffusion in silicon, *NASE-CODE VII*, Trinity College, Dublin, Ireland, Boole Press, 1991, pp. 15–17.
 - [36] S.M. Hu, Vacancies and self-interstitials in silicon: generation and interaction in diffusion, *J. Electrochem. Soc.: Solid-State Science and Technology*, 139(7) (1992) 2066–2075.
 - [37] E. Guerrero, H. Pötzl, R. Tielert, M. Grasserbauer and G. Stingeder, Generalized model for the clustering of As dopants in Si, *J. Electrochem. Soc.: Solid-State Science and Technology*, 129(8) (1982) 1826–1831.
 - [38] H.R. Soleimani, Modelling of high-dose ion implantation-induced dopant transient diffusion, and dopant transient activation in silicon (boron and arsenic diffusion), *J. Electrochem. Soc.: Solid-State Science and Technology*, 139(11) (1992) 3275–3284.
 - [39] Y. Tamaki, T. Shiba, T. Kure, K. Ohyu and T. Nakamura, Advanced process device technology for 0.3 μ m high-performance bipolar LSIs, *IEEE Trans. Electron Dev.*, 39(6) (1992) 1387–1391.
 - [40] F. Lau, Modelling of polysilicon diffusion sources, *IEDM Technical Dig.*, 90 (1990) 737–740.
 - [41] P. Pichler, *ICECREAM User's Guide 4.2*, 1990.
 - [42] S. Kalainathan, R. Dhanasekaran and P. Ramasamy, Grain size and size distribution in heavily phosphorus doped polycrystalline silicon, *J. Crystal Growth*, 104 (1990) 250–256.
 - [43] C.V. Thompson, Secondary grain growth in thin films of semiconductors: Theoretical aspects, *J. Appl. Physics*, 58(2) (1985) 763–772.
 - [44] O.C. Zienkiewicz, *The Finite Element Method*, Vol. 2, McGraw-Hill, 1991.
 - [45] D.L. Scharfetter and H.K. Gummel, Large-signal analysis of a silicon read diode oscillator, *IEEE Trans. Electron Dev.*, 16(1) (1969) 64–77.
 - [46] M.S. Mock, *Analysis of Mathematical Models of Semiconductor Devices*, Boole Press, Dublin, 1983.
 - [47] S. Selberherr, *Analysis and Simulation of Semiconductor Devices*, Springer, 1984.
 - [48] T.F. Chan and K.R. Jackson, Nonlinearly preconditioned Krylov subspace methods for discrete Newton algorithms, *SIAM J. Scientific and Statistical Computing*, 5(3) (1984) 533–542.
 - [49] W.E. Perry, *A Structured Approach to System Testing*, QED Information Sciences, 1988.
 - [50] R. Strasser, G. Nanz and W. Joppich, Process simulation for nonplanar structures with the multigrid solver LiSS, *SISDEP 93*, 1993, 201–204.
 - [51] O. Heinrichsberger, M. Thurner and S. Selberherr, Practical use of a hierarchical linear solver concept for 3D MOS device simulation, *SISDEP 93*, 1993, 85–88.
 - [52] A. Liegmann and W. Fichtner, The application of sparse supernodal factorization algorithms for structurally symmetric linear systems in semiconductor device simulation, *SISDEP 93*, 1993, 77–80.
 - [53] C.P. Ho, J.D. Plummer, S.E. Hansen and R.W. Dutton, VLSI process modeling – SUPREM III, *IEEE Trans. Electron Dev.*, 30(11) (1983) 1438–1453.

- [54] G. Hobler, S. Halama, K. Wimmer and H. Pötzl, RTA-simulations with the 2D process simulator PROMIS, *NUPAD III*, 1990, 13–14.
- [55] D.S. Boning, Semiconductor process design: representation tools, and methodologies, *PhD thesis*, Massachusetts Institute of Technology, 1991.
- [56] J.S. Wenstrand, *An Object-Oriented Model for Specification, Simulation, and Design of Semiconductor Fabrication Processes*, Technical Report ICL91-003, Integrated Circuits Laboratory, Stanford University, 1991.
- [57] Ch.J. Hegarty, *Process-Flow Specification and Dynamic Run Modification for Semiconductor Manufacturing*, Technical Report UCB/ERL M91/40, University of California, Berkeley, 1991.
- [58] J. Daniell and S.W. Director, An object oriented approach to CAD tool control, *IEEE Trans. Computer-Aided Design Integrated Circuits and Syst.*, 10(6) (1991) 698–713.
- [59] E.W. Scheckler, A.S. Wong, R.H. Wang, G. Chin, J.R. Camanga, A.R. Neureuther and R.W. Dutton, A utility-based integrated system for process simulation, *IEEE Trans. Computer-Aided Design Integrated Circuits and Syst.*, 11(7) (1992) 911–920.
- [60] A.S. Wong, Technology computer-aided design frameworks and the PROSE implementation, *PhD thesis*, University of California, Berkeley, 1992.
- [61] S. Halama, F. Fasching, C. Fischer, Ch. Pichler, H. Pimingstorfer, H. Puchner, G. Rieger, G. Schrom, T. Simlinger, H. Stippel, E. Strasser, W. Tuppa, K. Wimmer and S. Selberherr, The Viennese integrated system for technology CAD applications, *Technology CAD Systems*, 1993, 197–236.
- [62] Ch. Pichler and S. Selberherr, Process flow representation within the VISTA framework, *SISDEP 93*, 1993, 25–28.
- [63] S.G. Duvall, An interchange format for process and device simulation, *IEEE Trans. Computer-Aided Design Integrated Circuits and Syst.*, 7(7) (1988) 741–754.
- [64] S. Halama *et al.*, *VISTA Newsletter 5/93*, Internal document.